Digital holographic microscopy (DHM) using a Gaussian weighted sideband to reduce noise from DC spectrum

doi: https://doi.org/10.1109/ICTC52510.2021.9620964

Digital holographic microscopy (DHM) using a Gaussian weighted sideband to reduce noise from DC spectrum

Hyun-Woo Kim
Dept. of Computer Science and Networks
Kyushu Institute of Technology
Iizuka City, Fukuoka
kim@ois3d.cse.kyutech.ac.jp

Myungjin Cho
School of ICT, Robotics, and Mechanical Engineering, IITC
Hankyong National University
Anseong, Kyonggi-do, Republic of Korea
mjcho@hknu.ac.kr

Naoki Konishi
Dept. of Computer Science and Networks
Kyushu Institute of Technology
Iizuka City, Fukuoka
konishi@csn.kyutech.ac.jp

Min-Chul Lee
Dept. of Computer Science and Networks
Kyushu Institute of Technology
Iizuka City, Fukuoka
lee@csn.kyutech.ac.jp

***Abstract*— In a reconstruction of the 3D profile in digital holographic microscopy technology, there is a tradeoff relationship between detailed information of the target and the degree of noise depending on how wide the sideband of the Fourier domain is windowed. Besides, the conventional filtering method may not provide accurate height information because it filters using height information of surrounding pixels of the pixel to be filtered. For this reason, we propose a new filtering method that reduces noise by applying a Gaussian weighted windowed sideband in this paper. We compare the proposed filtering method with conventional filtering and verify the advantages and disadvantages of our method.**

Keywords*— *Image processing, Three-dimensional imaging, Noise reduction, Digital holographic microscopy,.

I. INTRODUCTION

Optical systems such as human eyes or image sensors can detect only the intensity of light, but they cannot detect phase information. For this reason, many researchers have used the interference characteristics of light to obtain the phase information of light. Holography is also one of the technologies for obtaining phase information of light by using the interference characteristics of light. Since holography was proposed in 1948 by Dennis Gabor, it has been researched in many branches by researchers [1]. After digital holography (DH) was proposed by Joseph Goodman in 1967 [2], the study of holography accelerated. Unlike conventional holography, which requires the use of special films, DH has the advantage of being able to use without significant limitations because it can be recorded using an image sensor. This technology is applied many research fields such as three-dimensional(3D) imaging [3], [4], 3D object recognition [5], 3D image encryption [6], [7], and digital holographic microscopy (DHM) [8]–[25], etc. Among the mentioned technologies, DHM is widely used in applications such as microstructure analysis [18]–[20], microbial research [21], [22], and diagnosis of diseases using cell analysis [23]–[25] due to the advantage of being able to obtain three-dimensional information of micro-objects. The image processing of DHM basically uses a method of obtaining 3D information of objects by using the frequency domain difference between the recorded reference image and the object image. In this processing, we have to select and window one of the sidebands in the Fourier domain to get the 3D information of the micro object. However, the frequency component of the sideband overlaps with the DC component in the Fourier domain of the recorded hologram. Thus, it is impossible to accurately window only the frequency component of the sideband. In addition, when the windowing range of the sideband is wide, the high-frequency is included. That is the detailed shape information of the target can be obtained. However, the noise of the DC component increases accordingly. On the other hand, when the windowing range of the sideband is narrowed, the noise due to the DC component is reduced. However, since only relatively low frequencies are included, the detailed shape information of the target is lost. To solve this tradeoff, we propose a normalized 2D Gaussian weighted windowed sideband. This is a method of reducing noise from the high-frequency region by making the windowed sideband with the same image size as the originally recorded hologram through zero paddings and multiplying the normalized Gaussian distribution. The proposed method is the principle of filtering by reducing the frequency component of the DC spectrum included in the windowed sideband. The conventional filtering methods such as Gaussian filter and median filter calculate the 3D profile for smoothing by using the value of the surrounding pixels of the filtering pixel. Therefore, it cannot be said to be accurate height information. In contrast, since the proposed method uses filtering in the Fourier domain, it can be said that it has more accurate height information compared to existing filtering methods. Furthermore, since our method filters after windowing the widest frequency range, there is also the expected effect that it can solve the problem of uncertainty about how wide the frequency range should be windowed to avoid noise in the DC spectrum.

This paper is organized as follows. In section 2, we explain the principle of the DHM and Gaussian weighted sidebands. Then, the experimental setup is described in section 3. We show the experimental results and a comparison with the conventional filtering method in section 4. In the final section, we discuss the effectiveness of our proposed method based on the experimental results.

II. THEORY

A. Digital Holographic Microscopy (DHM)

A conventional microscope provides only 2D shape information of microstructures. Thus, conventional microscopes are not suitable for obtaining 3D information of microstructures. Digital holographic microscopy (DHM) is proposed to supplement the limitation of the conventional microscope. As we mentioned earlier in section 1, DH is a technology that uses phase information that cannot be seen by using optical devices. DH uses the recorded interference pattern by two coherent lights to obtain phase information. Two coherent lights are called the reference beam and the object beam, respectively. The interference pattern recorded by the image sensor is expressed mathematically as follows [8], [20]:

$$I_H = |\boldsymbol{R}|^2 + |\boldsymbol{O}|^2 + \boldsymbol{R}^*\boldsymbol{O} + \boldsymbol{R}\boldsymbol{O}^* \quad (1)$$

$$= I_R + I_O + R^*Oe^{j(\phi_O-\phi_R)} + RO^*e^{-j(\phi_O-\phi_R)} \quad (2)$$

where I_H is the intensity of the hologram recorded by the image sensor, and $|R|^2 + |O|^2$ term is the DC spectrum of the recorded hologram. In addition, this term can be written as $I_R + I_O$. R and O are the complex amplitudes of reference and object, respectively, and A^* is the complex conjugate of A. Since in the $\phi_O - \phi_R$ term, ϕ_O and ϕ_R are phase information of object beam and reference beam, this term is a phase difference between these two beams. Moreover, this term can be derived as the following [8], [20]:

$$\phi_O - \phi_R = \Delta\phi(x,y) = \frac{2\pi}{\lambda}(n_t - n_s)h(x,y), \quad (3)$$

where λ is the wavelength of two coherent lights, and n_t and n_s are refractive indices of the target and surrounding media of the target, respectively. Besides, h is the height information of the target. To get the height information of the target, Eq. (3) can be changed as [8]:

$$h(x,y) = \frac{\Delta\phi(x,y)}{K \times \Delta n} \quad (4)$$

where K is the wavenumber. Therefore, by using Eq. (4), we can get the height information of the target. In the next section, we explain the problem in image processing of DHM and the proposed method.

B. DHM using a Gaussian weighted sideband

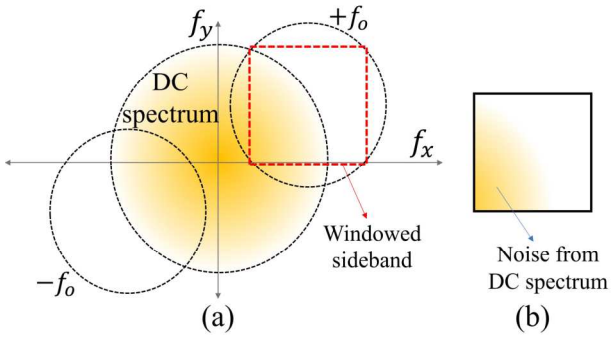

Fig. 1. Problem in image processing of DHM (a) windowing sidebands the 2D Fourier domain, (b) windowed sideband as red dashed square of (a).

To obtain $\Delta\phi$, we have to window the sideband in the Fourier domain of the recorded hologram.

Fig. 1 shows the problem in the image processing of DHM. Fig. 1 (a) shows the process of windowing sidebands in the Fourier domain. $\pm f_o$ of fig. 1 (a) denotes $R^*Oe^{j(\phi_O-\phi_R)}$ and $RO^*e^{-j(\phi_O-\phi_R)}$ in Eq. (2) for each sideband [20]. In fig. 1 (b), the windowed sideband has noise from the DC spectrum which increases as it approaches the origin in the Fourier domain. In this process, a high-frequency component of the object is required to obtain the detailed shape. Thus, the wide window is required. Furthermore, there is uncertainty for how wide sideband should be windowed to avoid noise in the DC spectrum. To solve this tradeoff, we propose a normalized 2D Gaussian weighted windowed sideband.

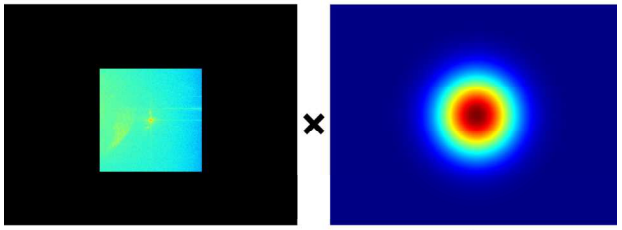

Fig. 2. Principle of the proposed method (a) windowed sidebands in the 2D Fourier domain and (b) 2D normalized Gaussian distribution.

Fig. 2 illustrates the principle of the proposed method. Fig. 2 (a) and (b) show the zero-padded windowed sideband and 2D normalized Gaussian distribution, respectively. By multiplying the windowed sideband by the normalized Gaussian distribution, noise included in the high frequencies area can be mitigated. The equation of the 2D Gaussian distribution drive as follows:

$$G_\sigma(x,y) = \frac{1}{\sqrt{2\pi}\sigma}e^{-\frac{x^2}{2\sigma^2}} \cdot \frac{1}{\sqrt{2\pi}\sigma}e^{-\frac{y^2}{2\sigma^2}}$$

$$= \frac{1}{2\pi\sigma^2}e^{\left(-\frac{x^2+y^2}{2\sigma^2}\right)} \quad (5)$$

where σ is the standard deviation of the Gaussian distribution. Then, $G_\sigma(x,y)$ is divided by the maximum value of $G_\sigma(x,y)$ for normalization. When σ increases, the effect of the filter decreases, and vice versa.

III. EXPERIMENTAL SETUP

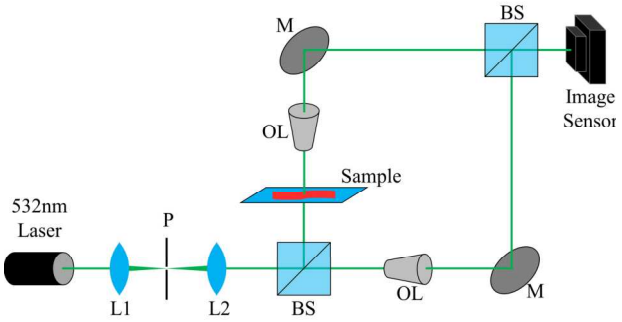

Fig. 3. Experimental setup. (L: lens, P: pinhole, M: mirror, BS: beam splitter, OL: objective lens)

In this paper, we use Mach-Zehnder interferometry to make the fringe pattern as narrow as possible. This is because the narrow fringe pattern makes the distance between the DC

spectrum and the sideband in the Fourier domain far. When the distance between each center of the sideband and the DC spectrum is far, as possible as wide sideband can be windowed.

Fig. 3 illustrates the experimental setup for the demonstration of our proposed method. The setup uses a 532nm laser diode module (3mW output power). A thin blood smear is used as a target. Both the object and the reference beams are magnified by a 40×(0.65 NA) objective lens. This experiment uses constant refractive indices of red blood cell (RBC) (n_t) and surrounding medium (n_s) with 1.42 and 1.34 (refractive index of the blood plasma), respectively [23]. Both holograms of the reference image and object image are recorded by CMOS sensor (Basler, acA2500-14uc, 2590 (H) × 1942 (V) pixel resolution) with a pixel size of 2.2 μm (H) × 2.2 μm (V). The beam splitter in front of the image sensor is tilted to make the fringe pattern as dense as the sampling criteria allow.

IV. Experimental Result

In this paper, we use a Goldstein phase-unwrapping algorithm for 3D profile reconstruction [26]. Authors and Affiliations

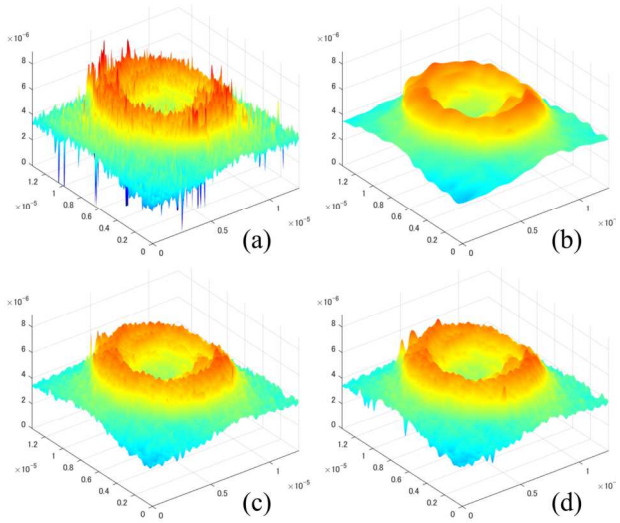

Fig. 4. Reconstructed 3D profile using (a) wide windowed sideband, (b) narrow windowed sideband, (c) proposed method, and (d) Gaussian filter ($\sigma = 2$) in (a), respectively.

Fig. 4 (a) and (b) show the 3D profile when windowed on a wide (800×800 pixels) area and a narrow (180×180 pixels) area, respectively. In addition, fig. 4 (c) shows the results of our proposed method. The applied σ value of the Gaussian weight is 130. The result by our proposed method has much less noise compared to the result by using the wide windowed sideband. However, there is no significant difference from the result by using Gaussian filtering ($\sigma = 2$) as shown in fig. 4 (d). Therefore, our method requires numerical comparison with Gaussian filtering. In this paper, we use the Signal to Noise Ratio (SNR) and Mean Square Error (MSE) to compare with the effectiveness of each filtering [27]. The smallest windowed sideband (fig.4 (b)) is used as a reference.

TABLE I. Comparison Result of SNR and MSE.

	Unfiltered	*Proposed method*	*Gaussian Filtering*
MSE	0.6090	0.2239	0.2122
SNR (dB)	20.9978	25.3440	25.5755

Table I shows the comparison results of SNR and MSE. From Table I, we can recognize that the effects of our proposed method and the Gaussian filter are similar without much difference. The result of the Gaussian filter has a slightly better result. We use statistical analysis since we cannot determine the effectiveness from only one target comparison. We randomly select 25 RBCs and their 3D profile using the same filtering process as fig 4.

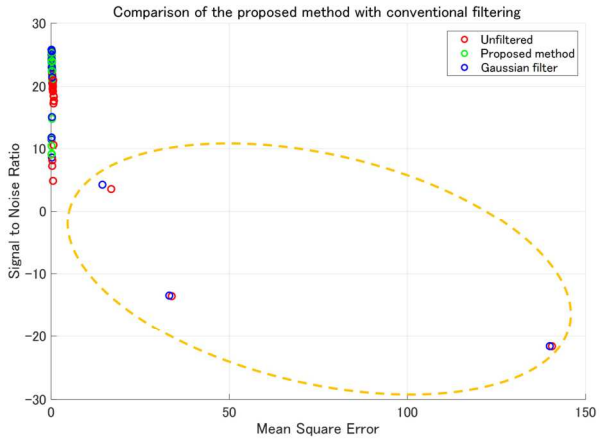

Fig. 5. Comparison result of randomly selected RBCs on the SNR-MSE coordinates

In fig. 5, the vertical and horizontal axes are the SNR value and the MSE value. Thus, coordinates in fig. 5 represent that the upper left is the high signal-low noise and the lower right is the low signal-high noise. However, it is difficult to compare the values of other points because the three pairs of points within the yellow dashed ellipse in fig. 5 are distributed over a wide range. These three pairs have a large MSE and small SNR because the noise is so great that the shape is seriously different with the reference 3D profile. However, our proposed method can recognize that these RBCs are also filtered and located in the upper left corner. For comparison excluding heavy noise cases, points located in the yellow dashed ellipse are excluded. Then, we compare them again.

TABLE II. Comparison Results of SNR and MSE by Statistical Analysis.

	MSE			*SNR (dB)*		
	UF	*PM*	*GF*	*UF*	*PM*	*GF*
S1	0.4662	0.19141	0.1669	18.5779	22.4438	23.0399
S2	0.4506	0.1882	0.1624	20.3080	24.1009	24.7392
⋮	⋮	⋮	⋮	⋮	⋮	⋮
S20	0.7665	0.2121	0.2929	18.4308	24.0105	22.6089
S21	140.5527	0.1197	139.9383	-21.6018	9.0949	-21.5828
S22	16.8800	0.2928	14.4045	3.5642	21.1720	4.2530
S23	33.8561	0.1352	33.1663	-13.5398	10.4460	-13.4504
S24	0.7867	0.2657	0.3367	17.7530	22.4678	21.4391
S25	0.6090	0.2239	0.2122	20.9978	25.3440	25.5755
avg	8.1258	**0.1977**	**7.6935**	13.9838	**20.5933**	**17.4684**
var	781.6978	**0.0023**	**776.4652**	115.0996	**30.0237**	**138.9112**

Table II shows the comparison result of SNR and MSE by statistical analysis, and Table III shows a modified version without three heavy noise samples. In Table II and III, UF is unfiltered, PM is our proposed method and GF is the Gaussian filtered 3D profile. As a result, our proposed method shows the high mean and low variance for both SNR and MSE. The low variance indicates the stability of filtering.

TABLE III. MODIFIED COMPARISON RESULTS OF SNR AND MSE BY STATISTICAL ANALYSIS.

	MSE			*SNR (dB)*		
	UF	***PM***	***GF***	***UF***	***PM***	***GF***
S1	0.4662	0.19141	0.1669	18.5779	22.4438	23.0399
S2	0.4506	0.1882	0.1624	20.3080	24.1009	24.7392
⋮	⋮	⋮	⋮	⋮	⋮	⋮
S20	0.7665	0.2121	0.2929	18.4308	24.0105	22.6089
Delete samples						
S24	0.7867	0.2657	0.3367	17.7530	22.4678	21.4391
S25	0.6090	0.2239	0.2122	20.9978	25.3440	25.5755
avg	0.5389	**0.1998**	**0.2195**	17.3260	**21.5509**	**21.2496**
var	0.0247	**0.0018**	**0.0046**	22.6954	**22.4956**	**22.8468**

Fig. 6 shows Table III displayed on SNR-MSE coordinates. As shown in fig.6, we can recognize that the Gaussian filter results are spread out more than the results of our proposed method. Therefore, it is noticed that our proposed method has the advantage of stably filtering regardless of the degree of the noise of the original hologram.

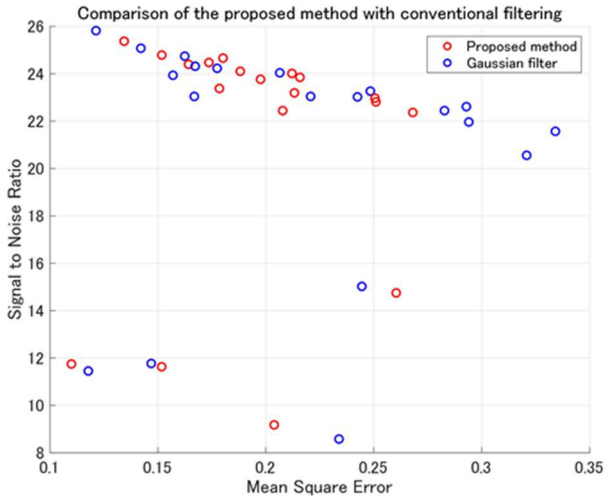

Fig. 6. Modified comparison results of randomly selected RBCs on the SNR-MSE coordinate.

V. CONCLUSIONS

In this paper, we have proposed a new filtering method to reduce the noise from the DC spectrum in DHM using a Gaussian weighted sideband. Then, we have compared our proposed method with Gaussian filtering methods. Our proposed method has shown strength in terms of stability regardless of the degree of the noise of the original hologram. Of course, if the σ of the Gaussian filtering changes, the filtering effect will be different. However, our proposed method can remove the noise while maintaining the detail of the target. Thus, we compared with the Gaussian filtering of σ which has similar effects to our proposed method. In addition, there is no uncertainty for the window size in our proposed method because the largest window size that can use the high frequency of the sideband can be used. Therefore, our proposed method is expected to be used when it is necessary to check the tendency of targets through multiple sampling.

ACKNOWLEDGMENT

This work was supported by the National Research Foundation of Korea(NRF) grant funded by the Korea government(MSIT) (NRF-2020R1F1A1068637).

REFERENCES

[1] D. Gabor , “Microscopy by reconstructed wave-fronts”, Proceedings of the Royal Society of London. Series A. Mathematical and Physical Sciences, vol. 197, no. 1051, pp. 454-487, 1949

[2] J. W. Goodman, and R. W. Lawrence, “Digital image formation from electronically detected holograms”, Applied physics letters, vol. 11, no. 3, pp. 77-79, 1967

[3] T. Tahara, X. Quan, R. Otani, Y. Takaki, and O. Matoba, “Digital holography and its multidimensional imaging applications: a review”, Microscopy, vol. 67, no. 2, pp. 55-67, 2018

[4] T. Tahara, A. Ishii, T. Ito, Y. Ichihashi, and R. Oi, “Single-shot wavelength-multiplexed digital holography for 3D fluorescent microscopy and other imaging modalities”, Applied Physics Letters, vol. 117, no. 3, pp. 031102, 2020

[5] U. Abeywickrema, R. Gnawali, P. Partha, and Banerjee, “Identification of 3D objects using correlation of holograms”, Applications of Digital Image Processing, vol. 10752, pp. 1075219, 2018

[6] N. Yu, S. Xi, X. Wang, L. Lang, X. Wang, L. Zhang, H. Han, Z. Dong, X. Jiao, and H. Wang, “Optical implementation of image encryption based on digital holography and computer generated hologram”, Journal of Optics, vol. 22, no. 7, pp. 075702, 2020

[7] S. K Rajput, and O. Matoba, “Optical multimodal biometric encryption that uses digital holography”, Journal of Optics, vol. 22, no. 11, pp. 115703, 2020

[8] A. Anand, V. Chhaniwal, and B. Javidi, “Tutorial: common path self-referencing digital holographic microscopy”, APL Photonics, vol. 3, no. 7, pp. 071101, 2018

[9] J. A. Picazo-Bueno, M. Trusiak, and V. Micó, “Single-shot slightly off-axis digital holographic microscopy with add-on module based on beamsplitter cube”, Optics Express, vol. 27, no. 4, pp. 5655-5669, 2019

[10] S. Shin and Y. Yu, “Lensless Reflection Digital Holographic Microscope with a Fresnel-Bluestein Transform”, Journal of the Korean Physical Society, vol. 74, no. 2, pp. 98-101, 2019

[11] T. O’Connor, A. Doblas, and B. Javidi, “Structured illumination in compact and field-portable 3D-printed shearing digital holographic microscopy for resolution enhancement”, Optics letters, vol. 44, no. 9, pp. 2326-2329, 2019

[12] Z. Zhong, H. Zhao, L. Cao, M. Shan, B. Liu, W. Lu, and H. Xie, “Automatic cross filtering for off-axis digital holographic microscopy”, Results in Physics, vol. 16, pp. 102910, 2020

[13] T. O’Connor, A. Anand, and B. Javidi, “Field-portable microsphere-assisted high resolution digital holographic microscopy in compact and 3D-printed Mach-Zehnder Interferometer”, OSA Continuum, vol. 3, no. 4, pp. 2326-2329, 2019

[14] J. Dong, A. K. Yetisen, X. Dong, F. Pöller, M. Jakobi, Z. Liu, F. Salazar Bloise, and A. W. Koch, “Low-pass filtering compensation in common-path digital holographic microscopy”, Applied Physics Letters, vol. 117, no. 12, pp. 121105, 2020

[15] L. Huang, L. Yan, B. Chen, Y. Zhou, and T. Yang : “Phase aberration compensation of digital holographic microscopy with curve fitting preprocessing and automatic background segmentation for microstructure testing”, OSA Continuum, vol. 462, no. 1, pp. 125311, 2020

[16] H. W. Kim, K. Inoue, M. Cho, and M. C. Lee, “A Study on Real-Time Modification of the Refractive Index of a Surrounding Medium using

a Uniform Microsphere in Digital Holographic Microscopy", Proceedings of the 2020 3rd International Conference on Electronics and Electrical Engineering Technology, pp. 44-48, 2020

[17] K. Inoue, A. Anand, and M. Cho, "Angular spectrum matching for digital holographic microscopy under extremely low light conditions", Optics letters, vol. 46, pp. 1470-1473, 2021

[18] B. Kemper and G. Bally, "Digital holographic microscopy for live cell applications and technical inspection", Applied optics, vol. 47, no. 4, pp. A52-A61, 2008

[19] T. Colomb, N. Pavillon, J. Kühn, E. Cuche, C. Depeursinge, and Y. Emery : "Extended depth-of-focus by digital holographic microscopy", Optics letters, vol. 35, no. 11, pp. 1840-1842, 2010

[20] S. Shin and Y. Yu, "Fine Metal Mask 3-Dimensional Measurement by using Scanning Digital Holographic Microscope", Journal of the Korean Physical Society, vol. 72, no. 8, pp. 863-867, 2018

[21] J. Zakrisson, S. Schedin, and M. Andersson, "Cell shape identification using digital holographic microscopy", Applied optics, vol. 54, no. 24, pp. 7442-7448, 2015

[22] D. Roitshtain, N. A. Turko, B. Javidi, and N. T. Shaked, "Flipping interferometry and its application for quantitative phase microscopy in a micro-channel", Optics letters, vol. 41, no. 10, pp. 2354-2357, 2016

[23] B. Javidi, A. Markman, S. Rawat, T. O'Connor, A. Anand, and B. Andemariam, "Sickle cell disease diagnosis based on spatio-temporal cell dynamics analysis using 3D printed shearing digital holographic microscopy", Optics express, vol. 26, no. 10, pp. 13614-13627, 2018

[24] T. O'Connor, A. Anand, B. Andemariam, and B. Javidi, "Deep learning-based cell identification and disease diagnosis using spatio-temporal cellular dynamics in compact digital holographic microscopy", Biomedical Optics Express, vol. 11, no. 8, pp. 4491-4508, 2020

[25] T. O'Connor, A. Anand, B. Andemariam, and B. Javidi, "Overview of cell motility-based sickle cell disease diagnostic system in shearing digital holographic microscopy", Journal of Physics : Photonics, vol. 2, no. 3, pp. 031002, 2020

[26] R. M. Goldstein, H. A. Zebker, and C. L. Werner, "Satellite radar interferometry: Two-dimensional phase unwrapping", Radio science, vol. 23, no. 4, pp. 713-720, 1988

[27] R. C. Gonzalez, and R. E. Woods, "Digital image processing", 2002